EUROPEAN ORGANIZATION FOR NUCLEAR RESEARCH
ORGANISATION EUROPEENNE POUR LA RECHERCHE NUCLEAIRE

CERN - PS DIVISION

PS/AE/Note 2001-017
PS/BD/Note 2001-012

MEASUREMENT OF OPTICAL AND BEAM PARAMETERS IN THE TRANSFER LINE TOWARDS THE DECELERATING RFQ

C. Bal, M. Giovannozzi, V. Prieto, U. Raich

Abstract

A number of beam profile measurements were performed in the transfer line delivering beam to the ASACUSA Decelerating RFQ (RFQD). The aim was to reconstruct the optical parameters and the beam emittance to verify whether the optics corresponds to the nominal one, and, eventually, to perform a new matching of the Twiss parameters. The ultimate goal was an overall increase of the deceleration efficiency of the RFQD. This note describes the instrumentation used to measure the beam profiles, the method applied to reconstruct the optical and beam parameters, as well as the experimental results.

Geneva, Switzerland
November 21 2001

1. Introduction

The deceleration efficiency of the RFQD used by the ASACUSA collaboration depends, among other parameters, upon the value of the optical functions, α, β, D, D', at its entry point. The perfect matching between the optical parameters of the transfer line and those needed by the RFQD was one of the issues in the design of the line (see Ref. [1] for more details). The computation of the optics of the transfer line was performed assuming some nominal values for the extraction parameters of the AD machine. In practise, those nominal values are not met, due to residual coupling effects (electron cooling) and also some stray fields present in the 7000 line. Hence, it is very likely that the Twiss parameters at the RFQD entry are different, albeit not very much, from the nominal ones.

The acceptance of the RFQD allows a certain tolerance in the values of α, β, D, D', and beam emittance, ε. This means that small deviations from their nominal values should not affect the deceleration efficiency. However, the decision has been taken to carry out a measurement campaign of the actual optics of the transfer line. This allows testing the difference between the nominal optics and the one presently used in operation in view of a possible rematching of the transfer line parameters. Of course, the ultimate merit-function for this procedure is the deceleration efficiency of the RFQD.

The determination of α, β, ε is obtained by means of beam profile measurements. This point is quite delicate in case of an antiproton beam of low-momentum (100 MeV/*c*) as is the case of the extracted beam from the AD machine.

Two different diagnostic systems are installed in the final section of the transfer line towards the RFQD:

- A couple of scintillating screens located in the same position as the monitors used for the watchdog system [1].
- Silicon strips detector [2], located in the same position as the second monitor of the watchdog system.

Both systems have been used for the measurements described in this note.

The plan of the note is the following: in section 2 the measurement devices are described in details, while in section 3 the method used together with the results obtained are presented. Finally some conclusions are drawn in the last section.

2 Beam Profile Measurements

2.1 Scintillating screens

2.2.1. Mechanical set-up

The assembly consists of two individual vacuum chambers, connected by a beam current transformer (see Fig.1). In the original design only tank 1 had a support while tank 2 was fixed to the transformer. This resulted in mechanical instability of the whole assembly. Any intervention on the transformer inevitably resulted in the necessity to re-align also the detectors installed in these tanks. To avoid this inconvenience, it was decided to modify the original layout and to provide also tank 1 with its own support.

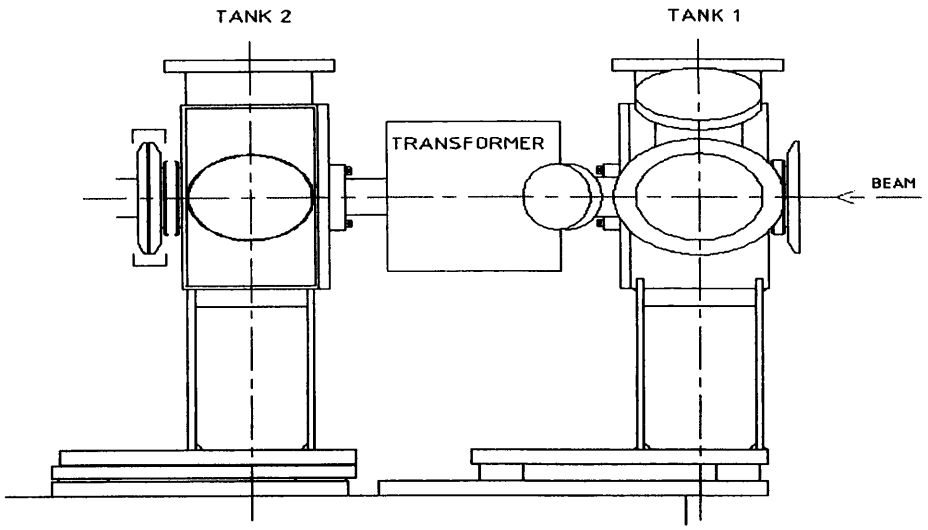

Figure 1: Mechanical layout of the two tanks.

The screens are named MTV70 and MTV75: MTV70 is mounted in the upstream tank 1, while MTV75 is located in the downstream tank 2. Each MTV has actually two screens observed by a single camera. The first one is mobile and it can be inserted in beam by means of a 24 V DC motor. It is oriented 45° with respect to the beam direction. The second one is fixed and it has a hole in its centre. It is located perpendicular to the beam axis to allow inserting other measurement devices whenever the mobile screen is not in use (see Fig. 2).

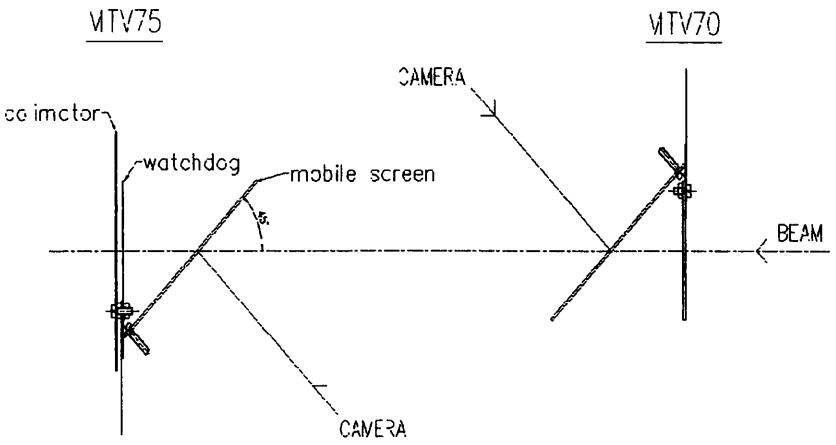

Figure 2: Mounting scheme.

The fixed screens are used as watchdog (see Ref. [1] for more details): any beam going through the two holes without intercepting the screens will fit entirely in the RFQD acceptance. The diameter of the hole is 21 mm and 14 mm for MTV70 and MTV75 respectively.

Calibration of the measurements is made possible by a grid engraved on the screen surface. The distortion introduced by the relative angle between the beam direction and the screen is directly taken into account by the grid. In fact, the horizontal step is $\sqrt{2}$ the vertical step size (see Fig. 3).

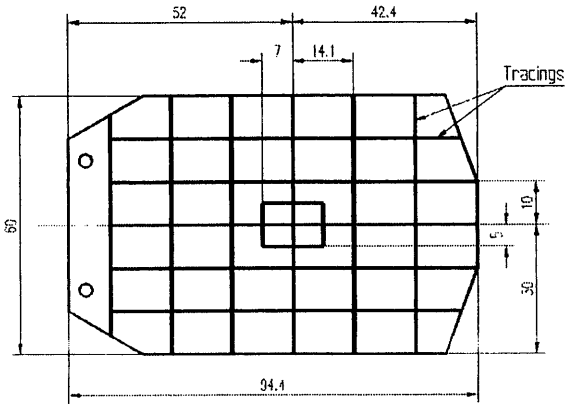

Figure 3: Details of the scintillating screen.

Special care was taken for the downstream screen. In fact, the tank is mounted close to a RF buncher that creates a large flow of electrons. These in turns generate light flashes thus perturbing the beam profile measurement. In order to prevent these electrons from reaching the scintillating screen a black-anodised metal sheet with thickness 0.5 mm has been mounted behind the fixed screen located in tank 2 (visible in Fig. 2).

2.1.3. Scintillating screen material

A sheet of doped Caesium Iodide, CsI (TI), 1 mm thick is used for the scintillating screens. CsI (TI) is a crystal with high density and Z value. It is known for its high resistance to thermal and mechanical shock due to the absence of a cleavage plane. It is relatively soft and plastic. CsI (TI) is soluble in water, although it is not hygroscopic in a classic sense: when in contact with materials to which water vapour can adhere, or when used in atmospheres with a high relative humidity, surface degradation can occur.

This material has the highest light output of all presently known scintillators, thus making it very attractive for measuring low intensity beams. Some properties of different crystals are listed in Table 1 (from Ref. [3]).

MATERIAL	ρ [g/cm^3]	EMISSION MAXIMUM [nm]	DECAY CONSTANT [μs]	n[1]	CONV. EFF.	HYGROSCOPIC
NaI(Ti)	3.67	415	0.23	1.85	100	yes
CsI(Ti)	4.51	550	0.6/3.4	1.79	45	no
CsI (Na)	4.51	420	0.63	1.84	85	slightly
CsI (undoped)	4.51	315	0.016	1.95	4-6	no

Table 1: Properties of scintillators materials.

[1] Refractive index.

2.1.3. Readout of TV images and data handling

Instead of providing simply the TV image of the beam spot, a system to digitise the image was installed. Therefore, an off-line analysis of the beam profiles is possible, thus allowing extracting relevant physical parameters (like average beam position and beam width). A TV frame grabber system was purchased. The choice was made for a Matrox Meteor II PCI card including driver software and an access library running on MS Windows-95. This permitted to install the card and its software on a standalone PC. Since the software package is incompatible with the Unix operating system this frame grabber cannot be used on the standard PS control system environment.

The frame grabber card can be used to digitise video images from colour video cameras and therefore contains 3 independent ADCs with associated memory to convert the red, green and blue (RGB) analogue signals coming from the camera. This feature allows to connect three black and white cameras, as long as they are strictly synchronised, to the three analogue input channels.

To insure a proper conversion of the image signals coming from the beam, whose frequency is asynchronous with respect to the camera's frame timing, it must be possible to re-synchronise the cameras and the frame grabber card to the beam. This is done with an external signal created by the standard AD timing system. However, it is worthwhile mentioning that such a re-synchronisation disturbs the TV monitors directly connected to the cameras, resulting in a temporarily random-vertically shifted image.

The frame grabber card came with an image acquisition library that was used for the development of the image-readout program. It is written in C++ and runs under Windows-95 in a standalone manner. On an external trigger the two camera frames are acquired and read out from the frame grabber. These images are displayed on the screen in a pseudo colour image, each colour representing a different light intensity.

Control buttons are available for

- Starting continuous acquisition
- Taking a single image
- Stopping data taking

Using the mouse it is possible to define an *area of interest,* a rectangle around the beam spot, which is used for calculation of the horizontal and vertical beam profiles (all pixels outside the area of interest are discarded).

In the *applications* pull-down menu a button for calibration is available. It opens a calibration window into which the centre position of the beam (in pixels) and the conversion factors (pixels to mm) can be specified. These calibration values are used for beam position and width calculations.

To give access to measurement results on a remote computer a *web server* has been installed such that the acquired images as well as the calculated beam positions and width can be displayed on any computer running a *web browser* (e.g. Netscape)

2.2 Silicon Strips detector

The detector consists of two identical vacuum assembly of a commercial silicon strip S2461 from Hamamatsu, one for each transverse plane. The overall detector was already reported in reference [2] except for the IN/OUT mechanism. The main parameters are given in Table 2 [4].

Parameter	Value	Unit
Chip Size	50×50	mm
Active Area	48×48	mm
Strip pitch	1000	μm
Number of Strips	48	
Number of readout strips	48	
Strip Width	900	μm
Strip Length	48000	μm
Max. leakage current	30	nA
Min. breakdown voltage	100	V
Strip Capacitance	40	pF
Max.full depletion voltage	75	V
Wafer thickness	300±15	μm

Table 2: Characteristics of the silicon Strip detector Model S2461 from Hamamatsu.

In the present configuration, the applied polarisation voltage is 15 V, which corresponds to a depletion layer of 210 μm. The antiproton range at 100 MeV/*c* is about 210 μm; hence, the maximum yield of hole-electron pairs is obtained.

Each strip current is integrated by means of a capacitance of 100 nF and the integrated signal is converted by a 15 bits ADC (LSB is estimated to be about 30 pC). Apart from profile measurements, the sum of all the acquired bits of a single beam profile allows to estimate the impinging p-bar intensity, after a proper absolute calibration has been carried out. The integration timing sequence, data conversion, multiplexing, and transmission are managed by a local processor [2]. The remote data collection, fit and display is done on a PC running a *LabView* application.

Each detector is moved in and out by a DC motorised linear displacement. An interlock system allows only one plane to be used at the same time. The overall mechanical system can be seen in Fig. 4 (left and right respectively).

Each chip has been aligned and the results of the survey is as follows:

- Horizontally, the beam centre is between strips 23 and 24.
- Vertically, the beam centre is between strips 13 and 14. This means that an overall displacement of about ten strips is present. Furthermore, the chip is tilted by about 2°.

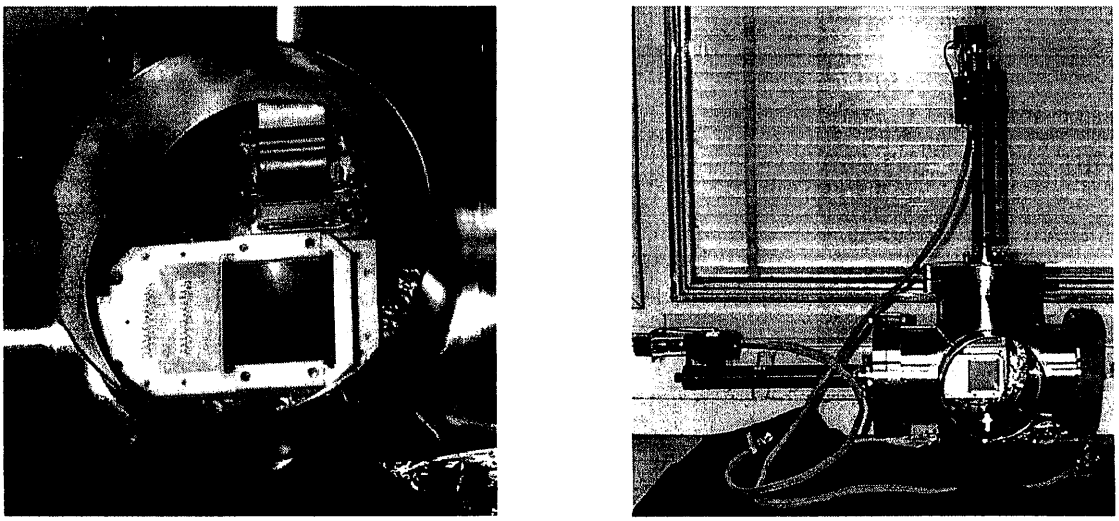

Figure 4: Micro Strip detector with support (left) and assembly tank with IN/OUT system (right).

3 Measurement of Optical and Beam Parameters

3.1 Beam Profile Analysis

The raw data, measured by means of the scintillating screens and silicon strips, have been analysed to extract the beam rms width used in the reconstruction of the Twiss parameters and emittance.

A fit procedure has been applied to each profile, the fit function being the sum of a gaussian and a constant, namely

$$f(x) = Ae^{\frac{(x-B)^2}{2C}} + D, \tag{1}$$

the fitted parameters being the amplitude A, the mean value B, and the rms value C, and the value of the constant function D. This choice allows the rejection of the pedestal in the beam profile. A first guess of the fitted parameters is obtained, and then a nonlinear minimisation routine is applied to compute the value of A, B, C, and D.

In Fig. 5 an example of raw beam profile, together with the fitted function is shown. The profile measured by means of the scintillating screen is shown on the left, while the one measured with the silicon strips is shown on the right.

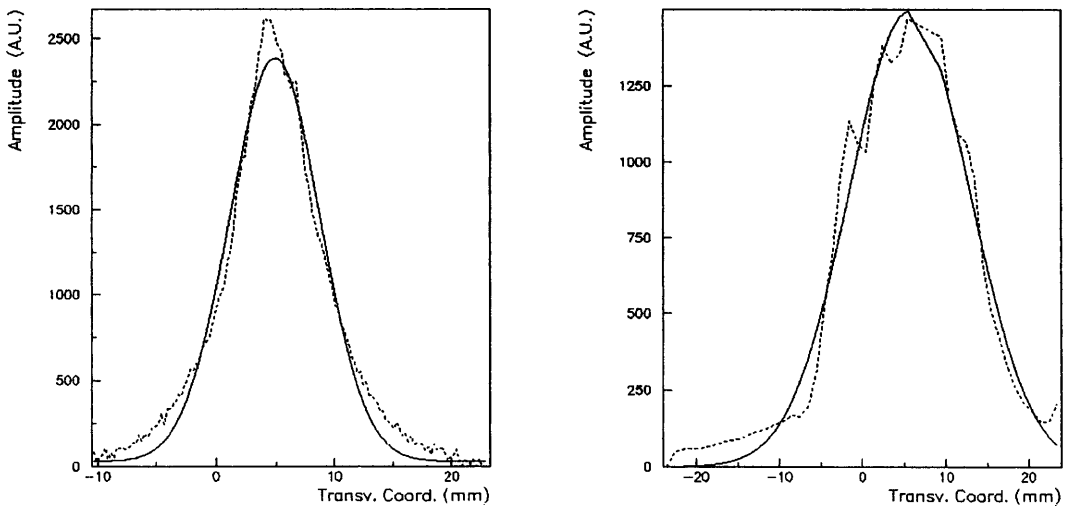

Figure 5: Vertical raw beam profile (dotted) and fitted function (solid). The profile measured by means of the scintillating screen is shown on the left, while the one measured with the silicon strips is shown on the right.

3.2 Reconstruction of Twiss Parameters and Emittance

Various methods can be used to reconstruct the Twiss parameters and the beam emittance from the knowledge of beam profiles [5]: The standard one is based on the analysis of three profiles located in a straight line. In this case, the dispersion function at the location of the three monitors has to be measured independently. More recently [6], new techniques have been proposed. Based on the knowledge of more than three profiles they allow the simultaneous measurement of Twiss parameters, beam emittance, together with dispersion function and its derivative. Unfortunately, all these techniques cannot be applied in the transfer line towards the RFQD. The three-profile method because the dispersion is quite difficult to be measured, while the new approach

requires many monitors and, in our case, only a very limited number of beam profile monitors are available.

For these reasons, a quadrupolar scan was applied. The beam size as a function of the gradient of a selected quadrupole, in our case DE1.QN50, was recorded. Under the assumption that the contribution of the dispersion function, via the beam momentum spread, to the measured beam size is negligible, this methods allows the reconstruction of α, β, ε.

This hypothesis is certainly true for the vertical plane. In the horizontal one the situation is different. For the nominal optics the final part of the transfer line is achromatic hence no coupling between transverse and longitudinal beam characteristics should occur. However, in reality the horizontal dispersion and its derivative are different from zero. Even in this case the assumption could be verified, at least in an approximate sense, thanks to the fact that the beam momentum spread is rather small and the term $D^2(\Delta p/p)^2$ is negligible with respect to the betatronic contribution given by $\beta\varepsilon$.

From the knowledge of the transfer matrix between the quadrupole and the monitor, the Twiss parameters at the monitor location can be expressed in terms of those at the entrance of the quadrupole, namely

$$\begin{pmatrix} \beta^i{}_m \\ \alpha^i{}_m \\ \gamma^i{}_m \end{pmatrix} = \begin{pmatrix} C^2{}_i & -2C_i S_i & S^2{}_i \\ C_i C'_i & C_i S'_i + C'_i S_i & -S_i S'_i \\ C'^2{}_i & -2C'_i S'_i & S'^2{}_i \end{pmatrix} \begin{pmatrix} \beta_q \\ \alpha_q \\ \gamma_q \end{pmatrix}, \tag{2}$$

where the subscript stands for the location (q for quadrupole, m for monitor) and the superscript refers to the i-th value of the gradient. The transfer matrix is expressed in the following form

$$M^i = \begin{pmatrix} C_i & S_i \\ C'_i & S'_i \end{pmatrix}. \tag{3}$$

The information concerning the optical parameters and beam emittance can be extracted from the different beam profile measurement by using a fitting procedure. The following function can be defined

$$\chi(\beta_q, \alpha_q, \gamma_q, \varepsilon; N) = \sum_{i=1}^{N} \left(\frac{\beta^i{}_m \, \varepsilon - \sigma_i^2}{\Delta\sigma_i^2} \right)^2, \tag{4}$$

where σ_i represents the measured beam size at the monitor location and $\Delta\sigma_i$ is the error associated with the measurement. Using Eq. (2) it is possible to express the value of the beta-function at the monitor location in terms of the Twiss parameters at the entrance of the quadrupole used in the scanning procedure and the elements of the transfer matrix (3). A least-square minimisation is applied to compute the following combinations of the free parameters, namely $\beta_q \varepsilon$, $\alpha_q \varepsilon$, $\gamma_q \varepsilon$. Using some little algebra, the Twiss parameters and the beam emittance can then easily disentangled.

At the same time, this technique allows to give estimates of the errors on the fitted parameters using the diagonal elements of the covariance matrix used in the least-square minimisation (see, for instance, Ref. [7] for more details). Of course, this approach is used both for horizontal and vertical planes.

3.3 Results

A series of fifteen beam profiles was taken, both in the horizontal and vertical planes, using the first scintillating screen and the silicon strips detector. Five values of the current of the quadrupole DE1.QN50 were used and for each value three beam profiles were recorded. This enables averaging the beam size for each value of the current, so that an estimate of the error can be associated to each measurement. To allow a direct comparison of the results obtained using the different detectors, a series of five profiles (one for each value of the current) were measured with the second scintillating screen, placed at the same location as the silicon strips.

In Fig. 6, the results of the beam profile measurements as functions of the quadrupole strength are reported. The horizontal plane is shown on the left, while the vertical one on the right.

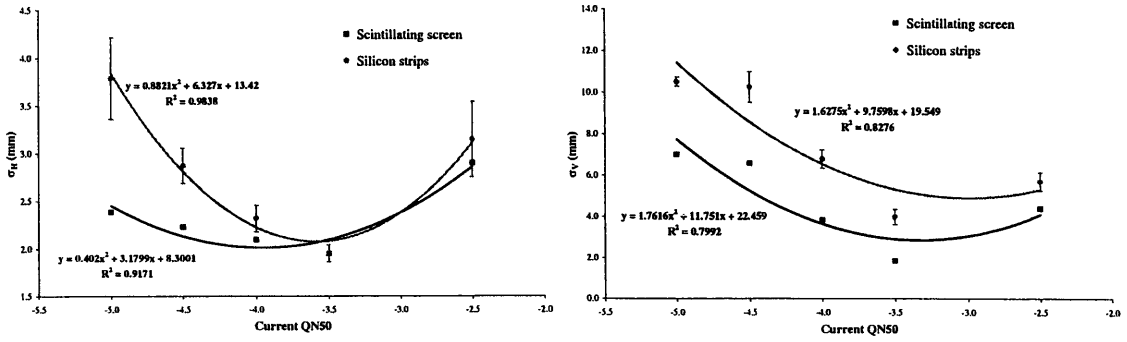

Figure 6: Beam size as a function of the current in the quadrupole DE1.QN50 as measured by the second scintillating screen and the silicon strips detector. The horizontal plane is shown to the left, while the vertical to the right. The error bars are obtained by averaging the beam size over the three profiles recorded.

In the horizontal plane the agreement between the two devices is quite remarkable. However, a substantial discrepancy is present in the vertical plane, where the silicon strips detector predicts a beam size systematically 1.5 larger than the one measured with the scintillating screen.

Using the measured values of the beam size together with the knowledge of the transfer matrix, computed using the *MAD* program [7], the reconstruction of the optical and beam parameters at the entrance of the quadrupole used for the scan was performed, according to the technique described in the previous section. The results are summarised in Table 3.

Plane	Device	α	$\Delta\alpha$	β [m]	$\Delta\beta$ [m]	ε (1σ) [π mm mrad]	$\Delta\varepsilon$ [π mm mrad]
Hor.	Scintillating screen 2	0.92	N.A.	2.26	N.A.	5.21	N.A.
	Silicon strips	0.72	0.39	3.36	1.43	8.27	2.80
Ver.	Scintillating screen 1	0.00	0.19	2.043	1.21	3.60	1.00
	Scintillating screen 2	-0.76	N.A.	8.63	N.A.	1.86	N.A.
	Silicon strips	-0.23	0.12	5.28	0.72	4.73	0.49

Table 3: Twiss parameters and beam emittance at the entrance of the quadrupole DE1.QN50 as measured with the scintillating screens and the silicon strips detectors. The errors on the fitted parameters are estimated using standard techniques based on covariance matrix associated with least-square minimisation.

Some comments can be made:

- The quality of the beam profiles measured with the first scintillating screen is not good enough to obtain meaningful results in the horizontal plane. In the vertical plane, however, it was possible to reconstruct a set of optical parameters.
- No error estimate on the fitted parameters is available for the results obtained from the second scintillating screen, as only one profile per current value was recorded.
- The reconstructed beam parameters obtained with scintillating screen and silicon strips are in reasonable agreement.
- The value of the vertical beam emittance shows a large difference: the value of ε_v reconstructed using the silicon strips is about 2.5 times larger than the one obtained with the scintillating screen. This is in agreement with the observation that the measured beam size is different.

Based on the previous set of measured data, it was possible to back-propagate the optical parameters at the beginning of the transfer line to determine the evolution of the Twiss functions along the line. In Fig. 7 the beta-function is shown from the exit of the horizontal bending magnet DE1.BHZ10 to the entry point of the RFQD. The different curves correspond to the different sets of initial parameters obtained using the various instruments. The results for both horizontal and vertical planes are presented.

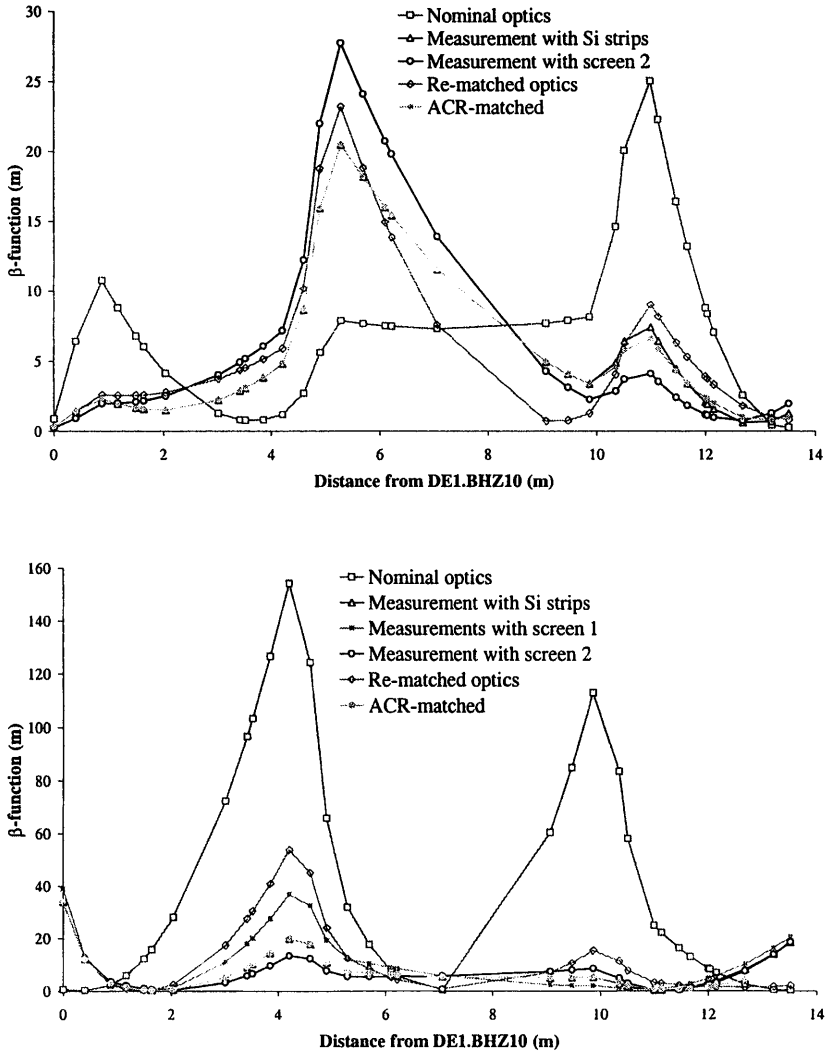

Figure 7: Evolution of the beta-function along the DE1 transfer line, from the bending magnet DE1.BHZ10 to the entry point of the RFQD. The upper plot shows the horizontal plane, while the lower one the vertical plane. Different curves are shown, referring to the different sets of initial conditions obtained by scintillating screens or silicon strips.

In the plots it is clearly visible that the initial conditions are quite different with respect to the nominal ones. The beta-function shows a remarkable agreement for all the sets of initial conditions reconstructed by means of the different detectors. Furthermore, it is also visible that at the entrance of the RFQD the beam is already divergent, while in the nominal optics it should be slightly convergent in both planes.

To improve this situation two different approaches have been tried:

- A new optics of the DE1 line has been computed using the *MAD* program and the measured set of initial conditions. The situation at the entrance of the RFQD could not be improved very much (see the corresponding curves in Fig. 7), as the beam is still quite divergent. This was also confirmed by a series of tests with beam.
- Using the nominal optics, the strength of the last two quadrupoles DE1.QN50 and DE1.QN60 was reduced to displace the location of the waist further downstream, near the entrance of the RFQD. This gave rather good results: this can be seen in the curve "ACR-matched" in Fig. 3, where the beta-function at the entrance of the RFQD is considerably reduced with respect to the original situation (about a factor of two).

The evolution of the alpha-function is presented in Fig. 8.

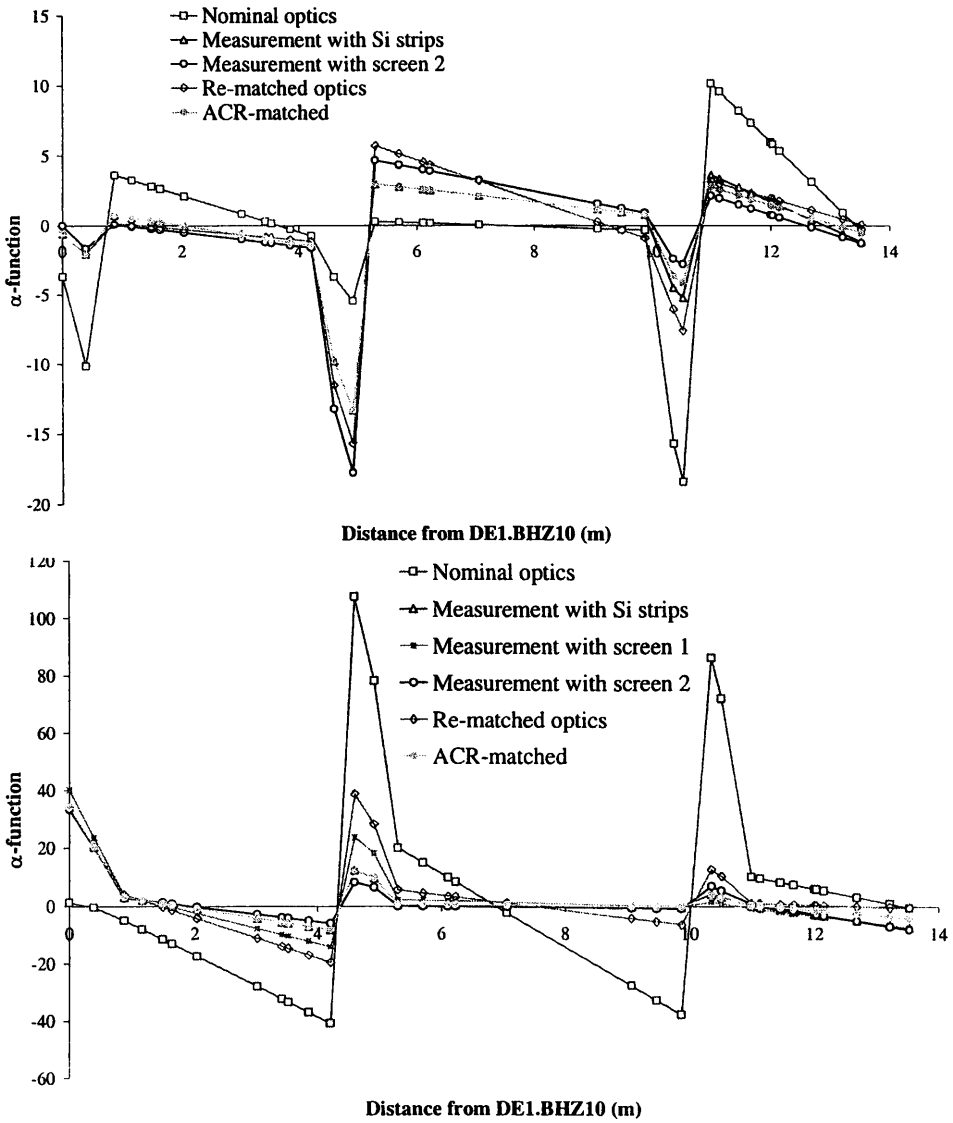

Figure 8: Evolution of the alpha-function along the DE1 transfer line, from the bending magnet DE1.BHZ10 to the entry point of the RFQD. The upper plot shows the horizontal plane, while the lower one the vertical plane. The different curves shown refer to the different sets of initial conditions obtained by scintillating screens or silicon strips.

4 Conclusion

In this note, the results of beam profile measurements performed using different devices, like scintillating screens and silicon strips, have been reported. The measurements were carried out using the low-momentum antiproton beam delivered by the AD machine. The aim was the reconstruction of the optical parameters of the transfer line delivering beam to the RFQD. To do this, an approach based on a quadrupole scan was used.

As a result, different sets of Twiss parameters have been obtained. They are in reasonable agreement and also, the evolution of the optical parameters along the transfer line is quite similar. These measurements showed that the optics is different with respect to the nominal one and, in particular, the beam at the entrance of the RFQD is divergent, while it should have been convergent.

Based on the measured initial conditions, different approaches have been applied to improve the situation, like rematching the optics using *MAD* or trying an empirical rematching. The latter proved to be the best strategy, allowing a reduction of the beta-function by almost a factor of two at the entrance of the RFQD.

Acknowledgements

We would like to thank E. Bravin, R. Maccaferri and G. Martini for their help, support, and discussions.

References

[1] J. Bosser et al., "Feasibility study of a decelerating Radio Frequency Quadrupole for the Antiproton Decelerator AD'', CERN PS Note 97-36 (HP), 1997.

[2] R. Maccaferri, "Tests of a Silicon Strip Beam Profile Monitor'', CERN PS Note 98-16 (BD), 1998.

[3] Table from NES technology S.A., Geneva.

[4] Hamamatsu Photonics, "Silicon Photodiodes and charge sensitive amplifiers for Scintillation Counting and High Energy Physics", p. 17, 1995.

[5] P. J. Bryant, K. Johnsen, "Circular Accelerators and Storage Rings'', Cambridge University Press, NY, 1993.

[6] G. Arduini, M. Giovannozzi. K. Hanke, D. Manglunki, M. Martini, "New Methods to Derive the Optical and Beam Parameters in Transport Channels'', Nucl. Instrum. Meth. A 459 16, 2001.

[7] W. H. Press, S. A. Teukolsky, W. T. Vetterling, B. P. Flannery, "Numerical Recipes in Fortran 77'', Cambridge University Press, NY, 1999.

[8] H. Grote, F. C. Iselin, "The *MAD* program – User's Reference Manual'', CERN SL 90-13 (AP), 1990.